



## Ofloxacin degradation over Cu–Ce tyre carbon catalysts by the microwave assisted persulfate process

Xiyang Liu<sup>a,1</sup>, Fei Huang<sup>b,1</sup>, Yang Yu<sup>a,c,\*</sup>, Peng Zhao<sup>a</sup>, Yuanbo Zhou<sup>a</sup>, Yide He<sup>a,c</sup>, Yanhua Xu<sup>a,c</sup>, Yongjun Zhang<sup>a,c,\*</sup>

<sup>a</sup> School of Environmental Sciences and Engineering, Nanjing Tech University, Nanjing 211800, China

<sup>b</sup> College of Pharmacy, Nanjing Tech University, Nanjing 211800, China

<sup>c</sup> NanjingTech Institute for ChemEng&Environ Materials, Nanjing Tech University, 211800, China



### ARTICLE INFO

#### Keywords:

Cu–Ce tyre carbon catalysts

Ofloxacin

Microwave assisted persulfate process

Degradation mechanism

### ABSTRACT

In this study, the degradation of ofloxacin (OFX) over Cu–Ce tyre carbon catalysts by the microwave assisted persulfate process was examined for the first time. The results showed that the Cu–Ce tyre carbon catalysts dramatically improved OFX decay efficiency. The optimal reaction conditions were the Cu–Ce tyre carbon catalysts of 2.0 g/L and the persulfate dosage of 12.0 g/L under microwave power of 400 W at 60 °C. The OFX conversion and total organic carbon (TOC) removal reached 95.8% and 87.6%, respectively, after 60 min catalytic oxidation under optimal conditions. To identify the properties of Cu–Ce tyre carbon catalyst, scanning electron microscopy (SEM), high-resolution transmission electron microscopy (HRTEM), the Brunauer–Emmett–Teller (BET), X-ray diffraction (XRD), X-ray photoelectron spectroscopy (XPS) and the ultraviolet-visible (UV-vis) diffuse reflectance spectra studies have been carried out. Eleven kinds of degradation products and five pathways during degradation process of OFX and degradation products were identified by GC–MS and HRMS.

### 1. Introduction

Antibiotics entering into environment, which are detrimental to human and environmental health, have attracted much attention recently [1,2]. As a second generation fluoroquinolone antibiotic, ofloxacin (OFX) has been widely used for treatment of bronchitis, pneumonia, chlamydia, gonorrhoea, skin infections, urinary and respiratory tract infections [3–5]. Significant concentration of OFX was detected in municipal wastewater treatment plant (53–1800 ng/L), hospital effluents (25000–35000 ng/L) and surface water (10–535 ng/L) [6–9] and can exist for a long periods of time [10]. It has been reported that traditional wastewater treatment technology, which including physical adsorption, chemical reactions, and biological degradation, are inefficient to eliminate antibiotics completely [11,12]. So, it is imperative to develop a method for effective removal OFX in wastewater.

Metal/metal oxides catalysts used in heterogeneous systems (e.g. Fe- [13], Co- [14], Mn- [15], and Cu-based [16] catalysts) have been broadly researched because they can be easily separated from the treated water for recycling. However, the cost of catalysts limited their application and it is necessary to prepare an effective catalyst with low price. As the tire industry continuously developing, waste tyres have

become a worldwide environmental problem [17,18]. Landfilling and being employed as additives in road pavement or in other applications are the most common disposal methods for used tyres [19]. However, these methods are not environmentally satisfactory as being non-biodegradable and may produce additional pollution, such as fire hazard and hence pose a serious air pollution problem [20]. Pyrolysis might be considered as an effective and environment-friendly recycling method which can convert waste tyres into activated carbon (TC) [18]. Common catalyst supports include activated carbon (AC) [21–23], coal carbon (CC) [24,25], TiO<sub>2</sub> [26–28] and diatomite [29–31]. The use of tyre carbon as catalyst support is a novel research area. One essential advantage of tyre carbon is its reliability that it is low cost. Compared with the commercial activated carbon (3000 \$/ton), the cost of tyre carbon is less than 120 \$/ton. Furthermore, waste tires are increasing quickly and tyre carbon has extensive sources. We find that the tyre carbon (TC) has high catalytic effect and could be employed as a cheap catalyst in advanced oxidation processes (AOPs).

In recent decades, advanced oxidation processes (AOPs), such as ozonation [32], Fenton [33], ultrasonic [34], photo-Fenton [35], photocatalytic [36,37] and persulfate oxidation processes [38,79], have been widely used in the removal of emerging contaminants in

\* Corresponding authors at: School of Environmental Sciences and Engineering, Nanjing Tech University, Nanjing 211800, China.

E-mail addresses: [yuyang19880421@yeah.net](mailto:yuyang19880421@yeah.net) (Y. Yu), [y.zhang@njtech.edu.cn](mailto:y.zhang@njtech.edu.cn) (Y. Zhang).

<sup>1</sup> These authors contributed equally to this work.

wastewater for their remarkable treatment efficiency [39]. Traditional Fenton reaction uses ferrous ions ( $\text{Fe}^{2+}$ ) as homogeneous catalysts to stimulate  $\text{H}_2\text{O}_2$  to generate hydroxyl radicals ('OH) [40,41]. However, the strict requirement for acidic conditions (pH 2–4), generation of large amount of chemical sludge and the leaching of metal ions limit its application in wastewater treatment [42–44]. As promising alternatives, sulfate radical-based AOPs has received more and more attention due to the convenience and stability of oxidants like persulfate [44].

The sulfate free radical ( $\text{SO}_4^{\cdot-}$ ) is a powerful one-electron oxidant with a high standard redox potential of 2.6 V [45] and also can react via electron transfer [77]. The sulfate free radical is able to oxidize most organic contaminants to  $\text{CO}_2$  and  $\text{H}_2\text{O}$  [45]. Different approaches have been used to activate persulfate to produce  $\text{SO}_4^{\cdot-}$ , such as UV irradiation [46,47], heating [48,49], ultrasound [50], base [51], phenols [52], quinones [53], metal ions [54,55]. Compared with common heating mode, microwave irradiation has a shorter reaction time, lower energy requirement and can increase the selectivity of reaction, improve the speed of reaction, and so on [56–58]. Thus, the Microwave (MW)-assisted reactions have gained popularity and the applications of MW have also been growing [59].

This work studied the effect of tyre carbon catalysts in OFX degradation reaction by the microwave assisted persulfate process. The influences of catalysts, microwave condition and persulfate condition were discussed. And the optimum conditions of temperature, microwave power, catalyst dosage and persulfate dosage were investigated. The possible intermediates and pathways during degradation process of OFX and degradation products were identified by GC-MS and HRMS.

## 2. Materials and methods

### 2.1. Materials and reagents

Waste tires were obtained from a car repair shop in Nanjing (China). Ofloxacin was obtained from Bomei company and oxone (potassium peroxyomonosulfate, PMS) was purchased from Aladdin company.  $\text{Cu}(\text{NO}_3)_2 \cdot 3\text{H}_2\text{O}$ ,  $\text{Ce}(\text{NO}_3)_3 \cdot 6\text{H}_2\text{O}$ , methanol (MeOH) and tert-Butanol (TBA) were purchased from Sinopharm Chemical Reagent Co., Ltd. 5,5-dimethyl-1-pyrroline N-oxide (DMPO),  $\text{CuO}_2$  and  $\text{CeO}_2$  were purchased from Macklin company. All reagents were used without further purification. To obtain the OFX solution (300 mg/L), 300 mg OFX weighed by a pallet counter balance was dissolved in 1 L deionized water. The deionized water was obtained from a pure water treatment system (EPED-Z1-30T). The microwave experiment used an MCR-3A atmospheric pressure microwave chemical reactor (China).

### 2.2. Catalysts preparation

After pulling out most of the steel wire, the used tires were broken into rubber blocks (4–5 cm). Then, the rubber blocks was placed in a low-temperature pyrolysis device at conditions that micro-negative pressure was 0.030 MPa and the reaction temperature was 350 °C. The pyrolysis carbon was obtained after the reaction. After processes of cooling, magnetic separation and grinding, the tire carbon (TC) was obtained.

$\text{Cu}(\text{NO}_3)_2 \cdot 3\text{H}_2\text{O}$  and  $\text{Ce}(\text{NO}_3)_3 \cdot 6\text{H}_2\text{O}$  were dissolved in an ethanol solution (the active component loading of the metal was 4.9% and 0.1 wt%, respectively). The tire carbon was immersed in the mixed solution for 2 h. Then the tire carbon was calcined at 500 °C for 4 h with a heating rate of 3 °C min<sup>-1</sup> and high pure nitrogen (99.999 wt%) flow of 500 mL min<sup>-1</sup>. The Cu-Ce-TC catalysts were obtained after cooled to room temperature.

In order to compare with the Cu-Ce-TC catalysts, Cu-TC (the active component loading of Cu was 5%) and Ce-TC (the active component loading of Ce was 5%) were prepared with same method. Cu-Ce-TiO<sub>2</sub>, Cu-Ce-CC, Cu-Ce-diatomite and Cu-Ce-AC were prepared with TiO<sub>2</sub>,

coal carbon, diatomite and activated carbon, respectively (the active component loading of Cu was 4.9% and Ce was 0.1%).

### 2.3. Characterizations

The surface morphology of the catalyst was observed by a field emission scanning electron microscope (SEM, HITACHI S4800). The particle of samples were determined by high-resolution transmission electron microscopy (HRTEM, JEOL JEM-2010 UHR). The BET surface areas, pore volumes and pore diameters of catalysts were determined using TriStar II 3020. The XRD diffraction patterns were obtained from XD6 X-ray diffractometer (Beijing General Instrument Co., Ltd) with monochromatic Co K $\alpha$  radiation ( $\lambda = 1.54056 \text{ \AA}$ ) at 36 kV and 20 mA in the 2 $\theta$  scan range of 10–80°. The valence states of elements in the Cu-Ce-TC catalyst were determined by X-ray photoelectron spectroscopy (Thermo K-Alpha XPS). To evaluate the catalyst stability, the concentrations of leached ions were measured using an inductively coupled plasma emission spectroscopy (ICP-OES, ICP-5000). Total organic carbon (TOC) was measured by TOC-L<sub>CPH</sub> (Shimadzu, Japan). The active radicals were detected using electron paramagnetic resonance (EPR, EMX-10/12, Bruker, Germany). The ultraviolet-visible (UV-vis) diffuse reflectance spectra of the catalysts were recorded by a UV-vis spectrophotometer (PerkinElmer Lambda 950).

### 2.4. Experimental set-up

The experiment was divided into two parts: adsorption experiment and degradation experiment. In the adsorption experiment, the catalysts dosage of TC and Cu-Ce-TC were 1 g/L. Solutions were sampled every 10 min and measured absorbance after filtration process with 0.45  $\mu\text{m}$  membrane. In the degradation experiment, the influences of catalysts, microwave condition and persulfate condition were determined. And the optimum conditions of temperature, microwave power, catalyst dosage and persulfate dosage were investigated. Temperature and microwave power were controlled by the MCR-3A atmospheric pressure microwave chemical reactor (China).

### 2.5. Analytical methods

The maximum absorption wavelength of OFX solution was 288 nm according to the scanning curve, which measured by UV-1900PC UV-vis spectrophotometer (AOE Instruments, Shanghai, China). The OFX conversion was calculated by the following formula (Eq. (1)):

$$\text{OFX conversion (\%)} = (C_o - C_1)/C_o \times 100 \quad (1)$$

where  $C_o$  is the initial absorbance of OFX solution,  $C_1$  is the absorbance of OFX solution at the reaction time (t). In order to prove the data that determined by the UV-vis spectrophotometer (UV-1900PC, AOE Instruments, China) is reliable, the concentration of OFX was also monitored by an HPLC system (Agilent 1260). The mobile phase was acetonitrile: 0.1% formic acid-water = 85:15 (v/v), the flow rate was fixed at 0.5 mL/min, the retention time was 10 min, detection wavelength was 288 nm and injection volume was 20  $\mu\text{l}$ .

GC-MS analyses used an Agilent model 7890 A Gas Chromatograph (GC), which was equipped with a model 5975C Mass Selective Detector and a capillary column (HP-5 ms, 30 m × 0.25 mm × 0.25  $\mu\text{m}$ , Agilent J&W GC Columns). The initial temperature was 40° and kept for 5 min, then increased 10 °C min<sup>-1</sup> to 200 °C, which was held for 10 min. Highresolution mass spectra (HRMS) were performed on an Agilent Accrurate-Mass Q-TOF LC/MS 6520 mass spectrometer with the electron spray ionization (ESI) mode.

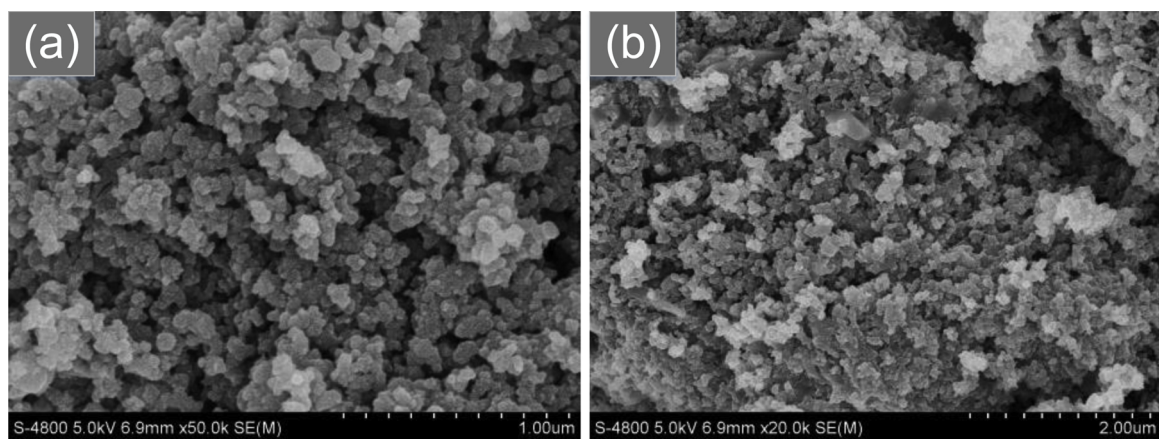


Fig. 1. SEM image of Cu-Ce-TC catalyst.

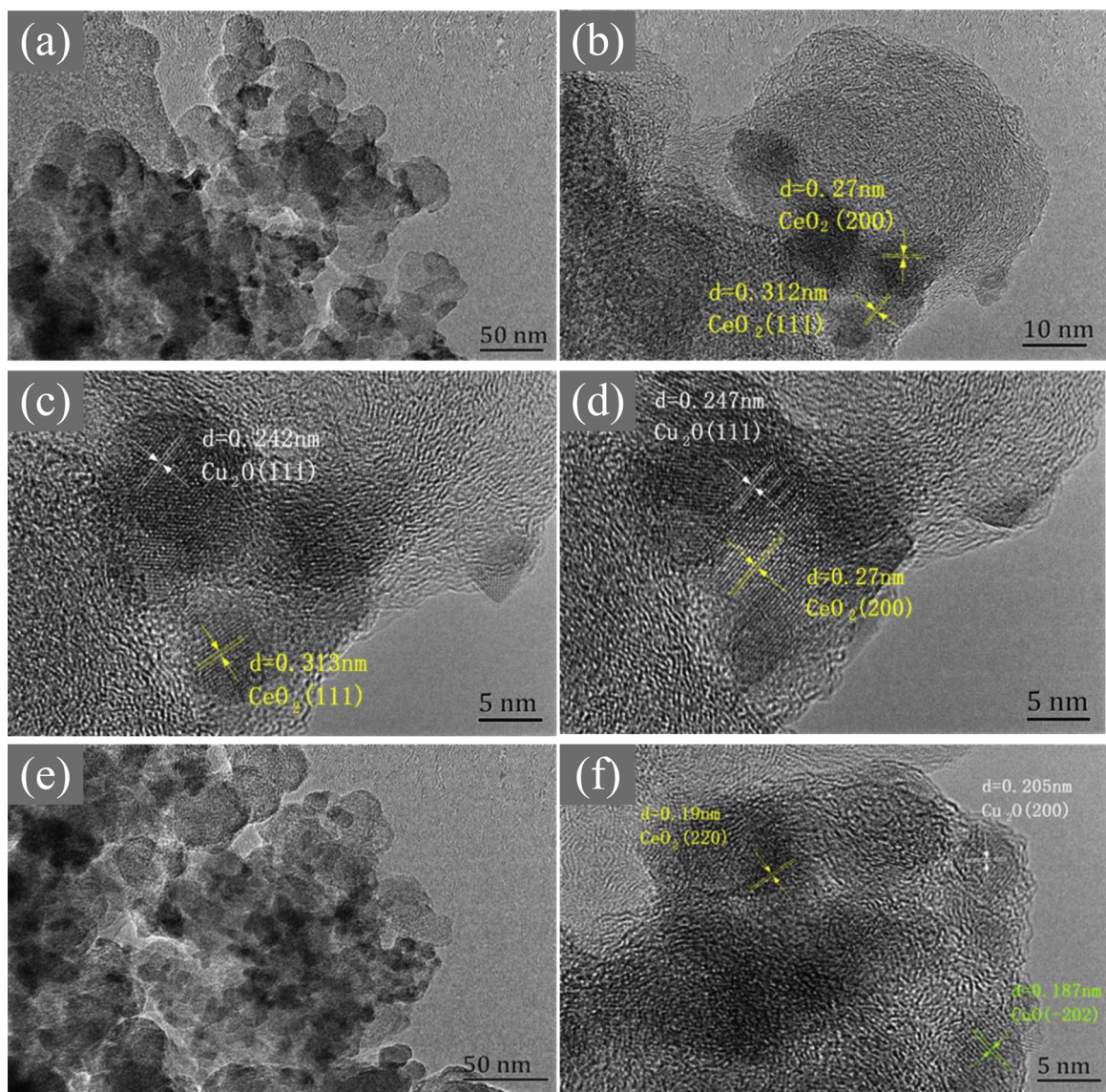
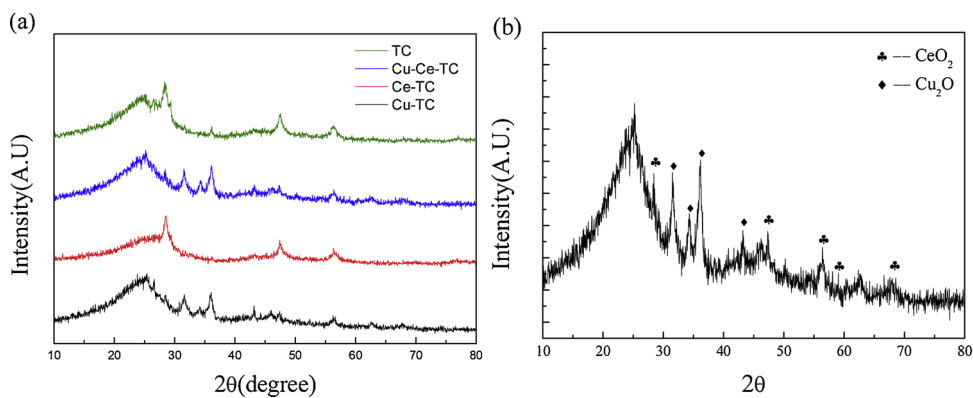


Fig. 2. HRTEM image of Cu-Ce-TC catalyst.



**Fig. 3.** XRD patterns of different catalysts (a) and XRD pattern of Cu-Ce-TC (b).

**Table 1**  
Specific surface area of two catalysts.

Catalysts	$S_{\text{BET}}(\text{N}_2)$ ( $\text{m}^2 \text{g}^{-1}$ )	Total pore volume ( $\text{cm}^3 \text{g}^{-1}$ )	Pore diameter (4 V/A)
TC	54	0.103	76.0
Cu-Ce-TC	129	0.123	43.2

### 3. Results and discussion

#### 3.1. Catalyst characterization

The SEM image of Cu-Ce-TC catalyst is presented in Fig. 1. It showed roughness surface with small spherical structure of different sizes. The

HRTEM image (Fig. 2) showed the existence of (111), (200) and (220) lattice fringes of cubic  $\text{CeO}_2$  with the interplanar spacing of 0.312 nm, 0.27 nm, and 0.19 nm, respectively. The existence of (111) and (200) lattice fringes of cubic  $\text{CuO}_2$  with the interplanar spacing of 0.242 nm, and 0.205 nm. The (−202) lattice fringes were cubic  $\text{CuO}$  and the interplanar spacing was 0.187 nm. The XRD patterns of the Cu-Ce-Tire carbon is shown in Fig. 3. The peak at  $2\theta = 28.54^\circ$ ,  $33.08^\circ$ ,  $47.48^\circ$ ,  $56.34^\circ$ ,  $59.09^\circ$  and  $69.41^\circ$  can be indexed to  $\text{CeO}_2$  (JCPDS 65–2975), and the peak at  $2\theta = 31.55^\circ$ ,  $34.32^\circ$ ,  $36.14^\circ$  and  $43.22^\circ$  can be indexed to  $\text{Cu}_2\text{O}$ .

The surface area, pore volumes and pore diameters of TC and Cu-Ce-TC catalysts are shown in Table 1. Cu-Ce-TC exhibited larger surface area ( $129 \text{ m}^2 \text{ g}^{-1}$ ) than TC ( $54 \text{ m}^2 \text{ g}^{-1}$ ). The total pore volume of TC and Cu-Ce-TC is  $0.103 \text{ cm}^3 \text{ g}^{-1}$  and  $0.123 \text{ cm}^3 \text{ g}^{-1}$ . The pore diameter

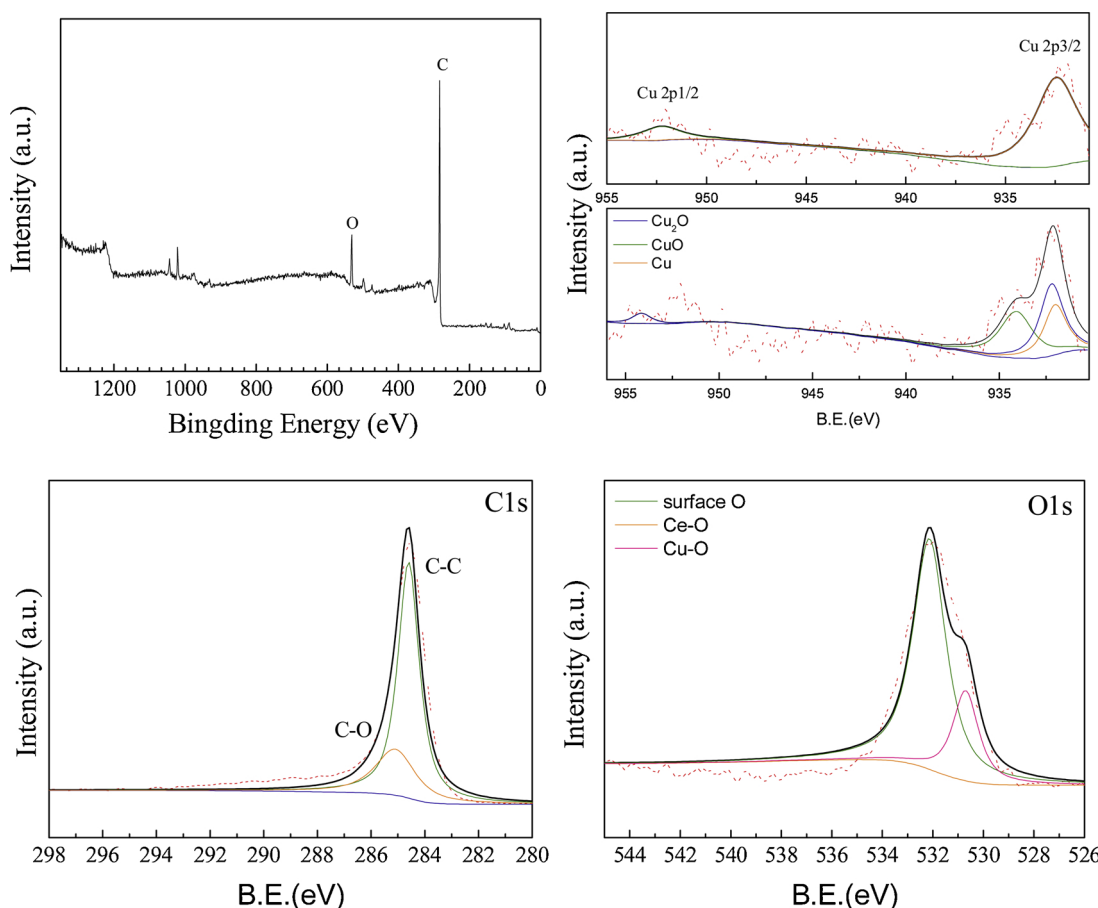


**Fig. 4.** Survey XPS spectra of Cu-Ce-TC (a), Cu 2p (b), C1s (c) and O1s (d) of Cu-Ce-TC.

**Table 2**

Deconvolution results of XPS spectra of Cu-Ce-TC.

Element	Peak	Position (eV)	FWHM (eV)	Area (%)
C	C–C	284.6	0.95	73.3
	C–O	285.1	1.78	26.7
O	surface oxygen	532.1	1.55	–
	Cu–O	530.7	1.22	–
	Ce–O	529.6	0.10	–
Ce	Ce 3d 3/2			–
	Ce 3d 5/2			–
Cu	Cu 2p 1/2	952.27	2.32	–
	Cu 2p 3/2	932.4	2.54	–
Cu	Cu	932.2	1.50	–
	CuO	954.1	0.50	–
		934.1	2.12	–
	Cu <sub>2</sub> O	932.0	1.46	–
		954.1	1.21	–

TC and Cu-Ce-TC is 76.0 4 V/A and 43.2 4 V/A, which indicated that Cu-Ce-TC has smaller pore diameter.

The XPS peaks of Cu-Ce-TC are shown in Fig. 4 and Table 2. The deconvolution of C1s spectra yielded the following two peaks: peak I (284.6 eV), carbon atoms in C–C; peak II (285.1 eV), carbon atoms in C–O. As shown in Table 2, the percentage of C–C and C–O is 73.3% and 26.7%. The deconvolution of O1s spectra yielded the following three peaks: peak I (532.1 eV), oxygen atoms in surface oxygen; peak II (530.7 eV) oxygen atoms in Cu–O; peak III (529.6 eV), oxygen atoms in Ce–O. The XPS Cu peaks of Cu-Ce-TC are presented in Table 2. The peak at 925.27 ev, 932.4 ev, 932.2 ev, 934.1–954.1 ev and 932.0–954.1 ev was assigned to Cu 3d 3/2, Cu 3d 5/2, Cu, CuO and Cu<sub>2</sub>O, respectively. The results are good agree with HRTEM and XRD analysis.

### 3.2. Adsorption experiment

#### 3.2.1. Comparison between UV-vis spectroscopy and HPLC

The experiment of comparison between UV-vis spectroscopy and HPLC was shown in Fig. S1 (Supporting information). The removal rate calculated by the area determined by the HPLC method was highly consistent with the removal rate calculated by the UV-vis spectroscopy, which proved the data that determined by the UV-vis spectrophotometer is reliable.

#### 3.2.2. Adsorption experiment

The adsorb ability of catalysts was tested at 20 °C. According to Fig. S2 (Supporting information), the adsorption removal of TC and Cu-Ce-TC was 1.1% and 4.1%, respectively. The adsorption of Cu-Ce-TC was higher than TC might due to larger surface area. But it should be noticed that the adsorption of ofloxacin by the two catalysts was weak, all lower than 5%, so the effect of adsorption on the experiment could be ignored.

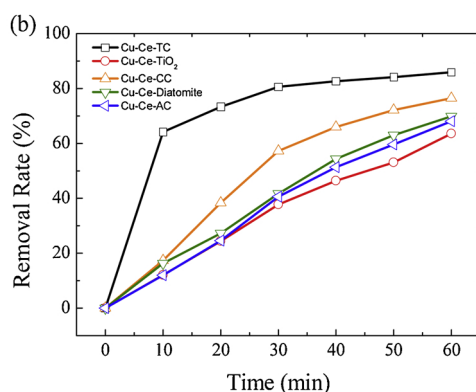
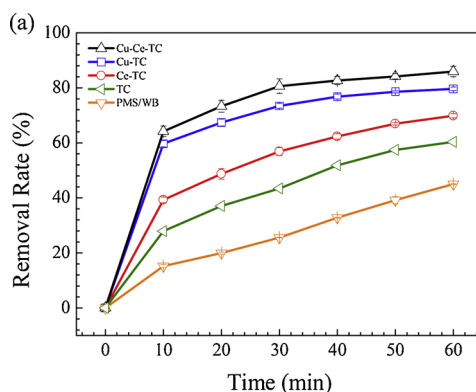


Fig. 5. The degradation curves of ofloxacin with different TC catalysts at 50 °C (a); the degradation curves of ofloxacin with different Cu-Ce catalysts at 50 °C (b).

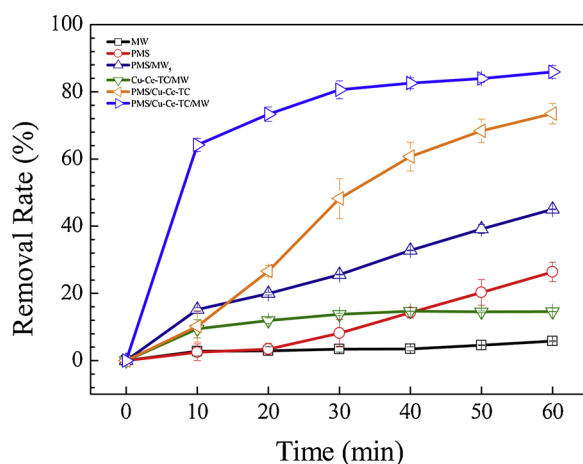


Fig. 6. The degradation curves of ofloxacin with different conditions at 50 °C.

### 3.3. Degradation of ofloxacin

#### 3.3.1. Comparison of different catalysts

The experiment of degrading OFX was performed at 50 °C, 400 W microwave power and 3 g/L persulfate and 1 g/L catalysts compare the catalytic activities of different catalysts. Samples were taken every 10 min to measure absorbance. As shown in Fig. 5(a), without catalyst, under the condition that 3 g/L persulfate and 400 W microwave power, the removal of OFX was 45.0% at 60 min. And the degradability of Cu-Ce-TC, Cu-TC, Ce-TC and TC at 60 min was 85.9%, 79.6%, 69.9% and 60.4% respectively. It was found that the catalytic performance of tire carbon increases after loaded metal. Interestingly, the tire carbon catalysts loaded with Cu and Ce (Cu-Ce-TC) have higher catalytic performance than the tire carbon catalysts that only loaded one kind of metal (Cu-TC, Ce-TC). The degradability of Cu-Ce-TC, Cu-Ce-TiO<sub>2</sub>, Cu-Ce-CC, Cu-Ce-diatomite and Cu-Ce-AC at 60 min was 85.9%, 63.6%, 76.5%, 69.9% and 68.0% respectively (Fig. 5(b)). The results showed that the tire carbon was the suitable and efficient support.

#### 3.3.2. Comparison of different reaction conditions

In order to investigate the effects of different reaction conditions in the degradation process of OFX, experiments on single conditions and combination conditions were studied at 50 °C. As shown in Fig. 6, under single conditions of 400 W microwave power (MW) and 3 g/L persulfate (PMS), the removal rate of OFX at 60 min was 5.8% and 26.4% respectively. Under combination conditions of 400 W microwave power and 3 g/L persulfate (PMS/MW), 400 W microwave power and 1 g/L Cu-Ce-TC catalyst (Cu-Ce-TC/MW), 3 g/L persulfate and 1 g/L Cu-Ce-TC catalyst (PMS/Cu-Ce-TC), the removal rate of OFX at 60 min were 45.0%, 14.6% and 72.6%, respectively. When the conditions combined

of 400 W microwave power, 3 g/L persulfate and 1 g/L Cu-Ce-TC catalysts (PMS/Cu-Ce-TC/MW), the reaction showed the fastest speed and the highest removal rate of 85.9% at 60 min. It indicated that Cu-Ce-TC catalysts can exhibit the highest activity by the microwave assisted persulfate process. Experiments on the effect of temperature, microwave power catalyst dosage and the effect of persulfate dosage were performed for further study the optimal conditions for the degradation of ofloxacin.

### 3.3.3. The effect of temperature

The effect of temperature on OFX conversion was studied under conditions that 400 W microwave power and 3 g/L persulfate and 1 g/L Cu-Ce-TC catalysts at temperatures of 30 °C, 40 °C, 50 °C and 60 °C. It is shown in Fig. 7(a) that after 60 min reaction, the removal rate of OFX at 30 °C, 40 °C, 50 °C and 60 °C was 52.9%, 76.8%, 86.0% and 89.9%, respectively. The degradation of OFX was fitted by a pseudo-first-order kinetic model [60,78]. As Fig. 7(b) and (c) shown, the pseudo-first-order rate constant ( $K_{obs}$ ) at 30 °C, 40 °C, 50 °C and 60 °C was 0.0026, 0.0053, 0.0218 and 0.0757, respectively. So,  $K_{obs}$  value was increased by 28-fold when the temperature was elevated from 30 to 60 °C [60]. The results were consistent with previous reports, indicated that high temperature could accelerate the decomposition rate of PMS, thus improve the degradation of OFX by the microwave assisted persulfate process with Cu-Ce-TC catalyst.  $K_{obs}$  (the pseudo-first-order rate constant) was obtained by linear regression of  $\ln [OFX]$  to time at each

condition (Eq. (2)) [61].

$$\ln\left(\frac{[OFX]_t}{[OFX]_0}\right) = -k_{obst} t \quad (2)$$

In addition, evaluated the temperature-dependence of  $K_{obs}$  was based on Arrhenius equation (Eq. (3)) [61].

$$\ln K_{obs} = \ln A - \frac{E_a}{RT} \quad (3)$$

where A is the pre-exponential factor,  $E_a$  is the apparent activation energy, R is the universal gas constant ( $8.314 \text{ J mol}^{-1} \text{ K}^{-1}$ ), and T is the absolute temperature [61]. As was shown in Fig. 7(d), a linear relationship ( $R^2 = 0.979$ ) could be established between  $\ln K_{obs}$  and  $1/T$  (T, the absolute temperature (K)). The apparent activation energy  $E_a$  ( $\text{kJ mol}^{-1}$ ) was  $101.7 \text{ kJ mol}^{-1}$  evaluated by linear regression using Arrhenius equation.

### 3.3.4. The effect of microwave power

The effect of microwave power on OFX conversion was studied under conditions that 50 °C, 3 g/L persulfate and 1 g/L Cu-Ce-TC catalysts at microwave power of 100 W, 200 W, 300 W and 400 W. According to Fig. 8(a), the removal rate of OFX in 100 W, 200 W, 300 W and 400 W, was 78.7%, 82.3%, 85.9% and 79.8%, respectively. It was found that compared with the effect of temperature, microwave power had a weaker effect on the degradation of ofloxacin. The reaction

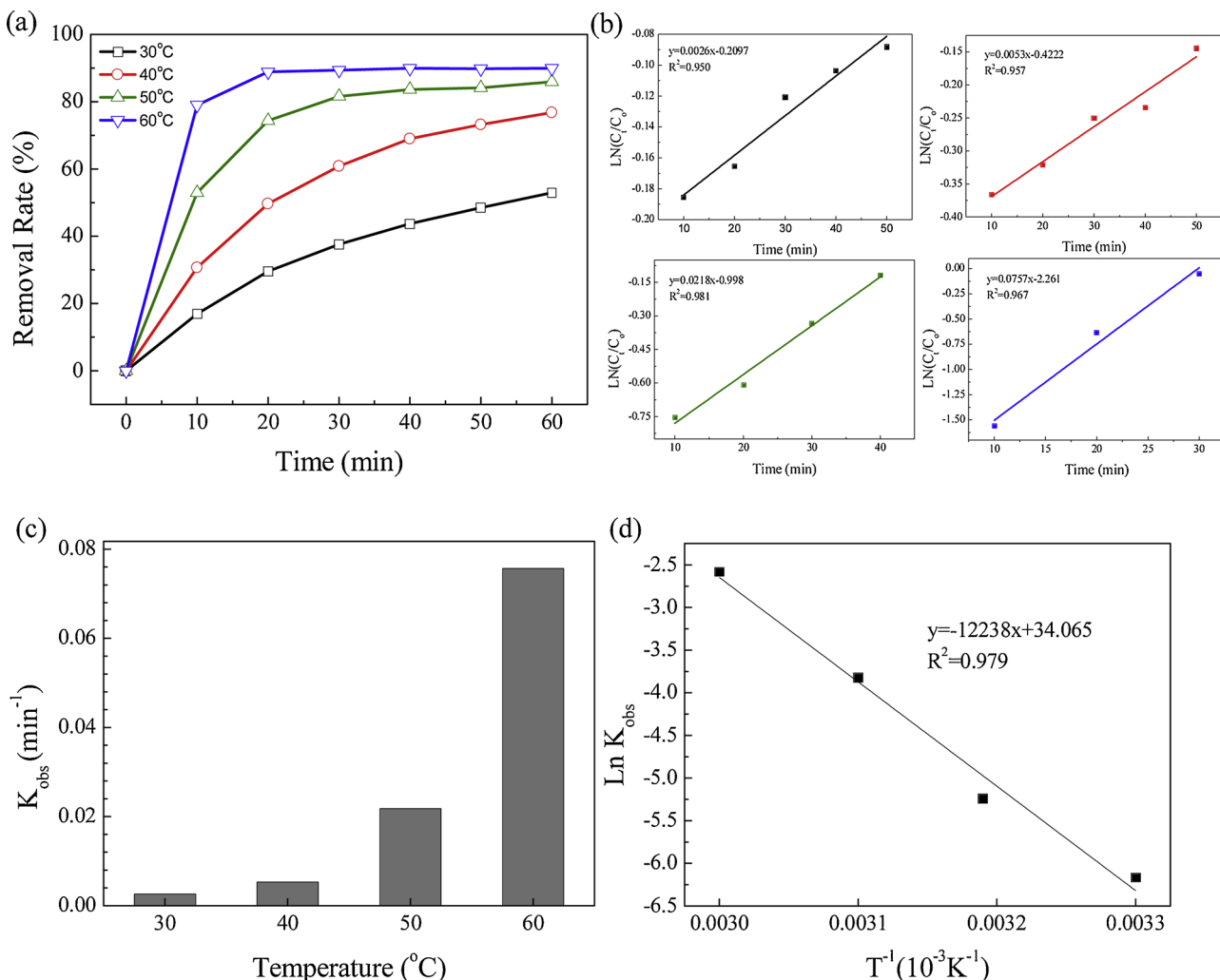


**Fig. 7.** Effects of temperature on ofloxacin conversion (a); Effects of temperature on the pseudo-first-order rate constant ( $K_{obs}$ ) (b) and (c); plot of  $\ln K_{obs}$  versus  $T^{-1}$  for  $E_a$  calculation via Arrhenius equation (d).

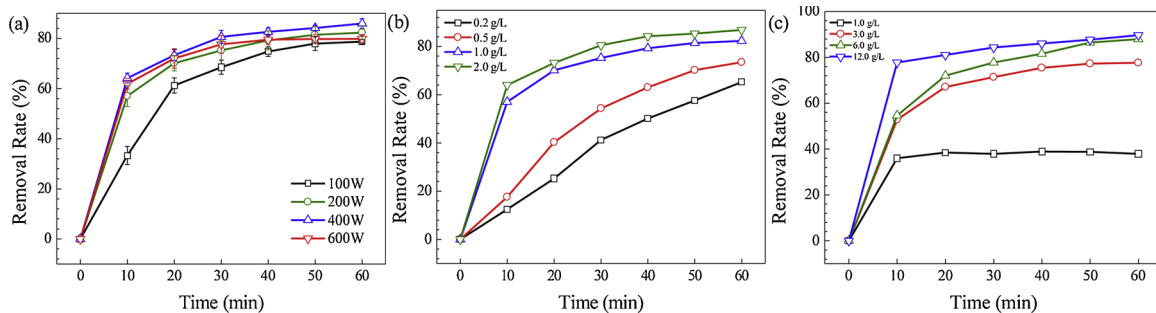


**Fig. 8.** Effect of microwave power on ofloxacin conversion (a), Effect of catalyst dosage on ofloxacin conversion (b), Effect of persulfate dosage on ofloxacin conversion (c).

rate increased as the microwave power from 100 W to 400 W, however, the removal rate of ofloxacin decreased under too high microwave power conditions (600 W). It is essential to optimize the microwave power so as to avoid unnecessarily excessive consumption of energy. Thus, microwave power of 200 W is used in subsequent experiments.

### 3.3.5. The effect of catalyst dosage

The effect of catalyst dosage on OFX conversion was studied at 50 °C under conditions that 200 W microwave power, 3 g/L persulfate and Cu-Ce-TC catalysts of 0.2 g/L, 0.5 g/L, 1 g/L and 2 g/L. From Fig. 8(b), the removal rate of OFX with 0.2 g/L, 0.5 g/L, 1 g/L Cu-Ce-TC catalysts was 65.2%, 73.5%, 82.3% at and 86.9%, respectively. It can be observed that the higher Cu-Ce-TC catalyst dosage resulted in higher removal efficiency.

### 3.3.6. The effect of persulfate dosage

The effect of catalyst dosage on OFX conversion was studied at 50 °C under conditions that 200 W microwave power, 1 g/L Cu-Ce-TC catalysts and persulfate of 1.0 g/L, 3.0 g/L, 6.0 g/L and 12.0 g/L. According to data in Fig. 8(c), the removal rate of OFX with 1.0 g/L, 3.0 g/L, 6.0 g/L and 12.0 g/L persulfate was 37.9%, 77.6%, 88.0% at and 89.7%, respectively. As the persulfate increased from 1.0 g/L to 3.0 g/L, the removal rate of OFX increased about 40%, while the persulfate increased from 6.0 g/L to 12.0 g/L only increased 2%.

### 3.3.7. Catalyst activity and stability

The activity and stability of Cu-Ce-TC catalyst was investigated by a five-cycle degradation of OFX under the same operating conditions. The reusability is vital factor that influencing practical application of Cu-Ce-TC catalyst in wastewater treatment. As shown in Fig. 9, with the increase in the number of uses, the catalytic activities decreased slightly,

which might due to the poor stability of Cu<sub>2</sub>O that reported in previous researches [62]. The ICP (Inductive Coupled Plasma Emission Spectrometer) was used to determinate of ions in the treated water and the result was 77.2 ppm copper ions and 1.4 ppm cerium ions.

### 3.3.8. Intermediate products and transformation pathways

In order to investigate the possible intermediates and pathways during degradation process of OFX, GC-MS and HRMS were used to identify degradation products. As shown in Fig. 10, eleven kinds of degradation products were identified in the degradation process. On the basis of results, five possible degradation pathways of OFX using Cu-Ce-TC were proposed. A previous study by Taicheng An et al reported that the partial and complete elimination of piperazinilic ring was observed in a degradation pathway (I) of fluoroquinolones [78]. OFX may loss of 1,4-dimethylpiperazine and demethylation firstly to form A\*, which may further be oxidized to G\*. Based on the previous study, the first addition position of the ·OH radical probably takes place on the quinolone ring [77]. C\* may be formed via attack of ·OH on heterocyclic ring-4. I\* was formed via cleavage of C—C bond and loss of the hydroxyl group form the heterocyclic ring-3 of C. In addition, OFX may produce B\*, H\* and E\* after decarboxylation. E\* may generated F\* because ·OH attack at the quinolone moiety of OFX. K\* might formed from F\* after the cleavage of the double-bonded side chain on the ring-3 structure of OFX molecule with a keto group. Consistent with the previous report, cleavage products D\* might formed after the loss of C<sub>11</sub>H<sub>15</sub>FN<sub>2</sub> [63]. J\* was generated by again oxygen atom removal from D\*. These products may further scission to naphthal ring opened products and finally degraded into H<sub>2</sub>O and CO<sub>2</sub>.

### 3.3.9. Proposed mechanism of persulfate activation on Cu-Ce-TC

From the above analysis and catalytic experiments, it can be seen that the Cu-Ce-TC performed better than Cu-TC and Ce-TC. In the mechanistic study, PMS can be activated to generate free radicals to oxidize organic contaminants. Quenching test by radical scavengers, a reliable method, was used to identify reactive oxidative species [64]. In PMS activation, SO<sub>4</sub><sup>·-</sup> and ·OH are often considered as reactive species for pollutant oxidation. According to different reaction rate with radicals, methanol (MeOH) can capture both ·OH and SO<sub>4</sub><sup>·-</sup> effectively ( $k_{SO_4^{·-}} = 1.1 \times 10^7 M^{-1} s^{-1}$ ,  $k_{·OH} = 9.7 \times 10^8 M^{-1} s^{-1}$ ) while tert-butyl-alcohol (TBA) prefers capturing ·OH rather than SO<sub>4</sub><sup>·-</sup> ( $k_{·OH} = 6 \times 10^8 M^{-1} s^{-1}$ ) [64]. Thus, the dominant reactive radical species in OFX degradation could be well distinguished according to the inhibition effects on reaction. As shown in Fig. 11(a) and (b), the existence of MeOH or TBA inhibited the degradation of OFX at different molar ratio with PMS. Compared with original reaction solution,  $k_{obs}$  showed dramatic decrease from  $0.0307 \text{ min}^{-1}$  to  $0.0049 \text{ min}^{-1}$  ( $n [MeOH/PS] = 400$ ) and  $0.0249 \text{ min}^{-1}$  ( $n [TBA/PS] = 400$ ), respectively (Fig. 11(d)). In addition, as shown in Fig. 11(c), compared with that of MeOH, the inconspicuous decrease of the degradation efficiency ( $n [TBA/PS] = 400$ ) might indicate the minor role of ·OH in the degradation process. These results suggest that both SO<sub>4</sub><sup>·-</sup> and ·OH were

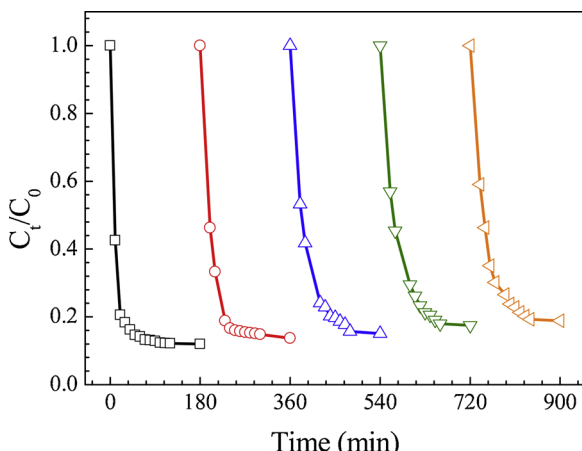


**Fig. 9.** Five cycles of degradation of OFX using Cu-Ce-TC catalyst by the microwave assisted persulfate process.

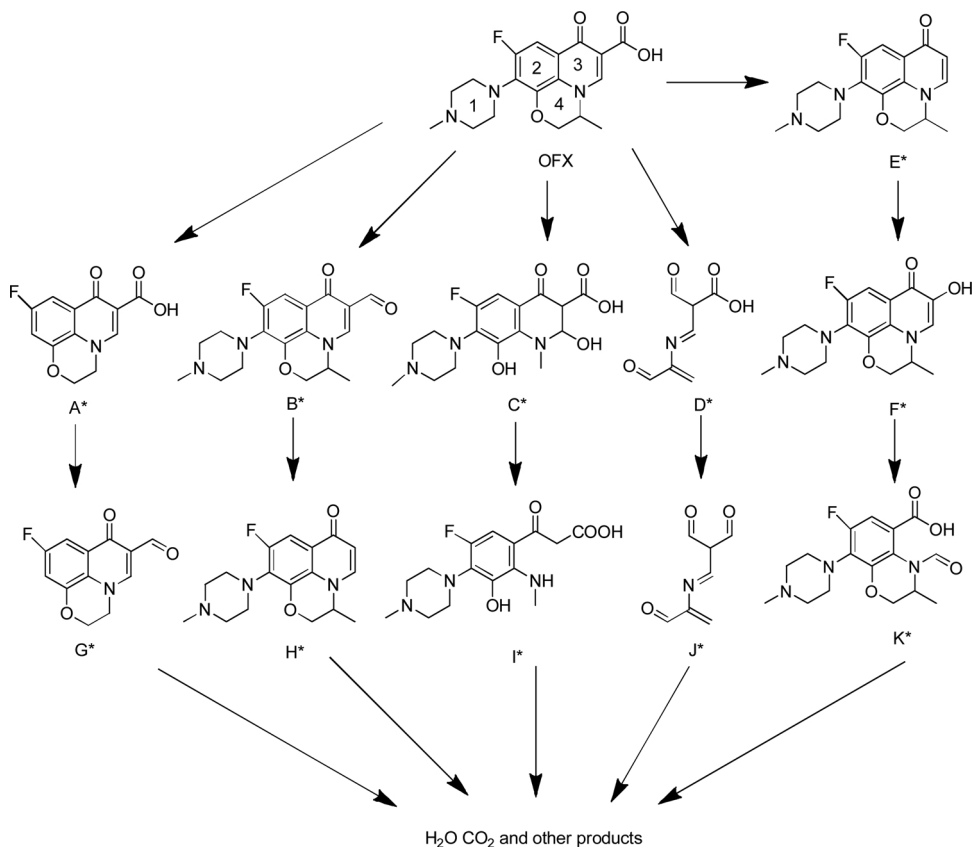


**Fig. 10.** Proposed pathways for OFX during the microwave assisted persulfate process with Cu-Ce-TC catalyst.

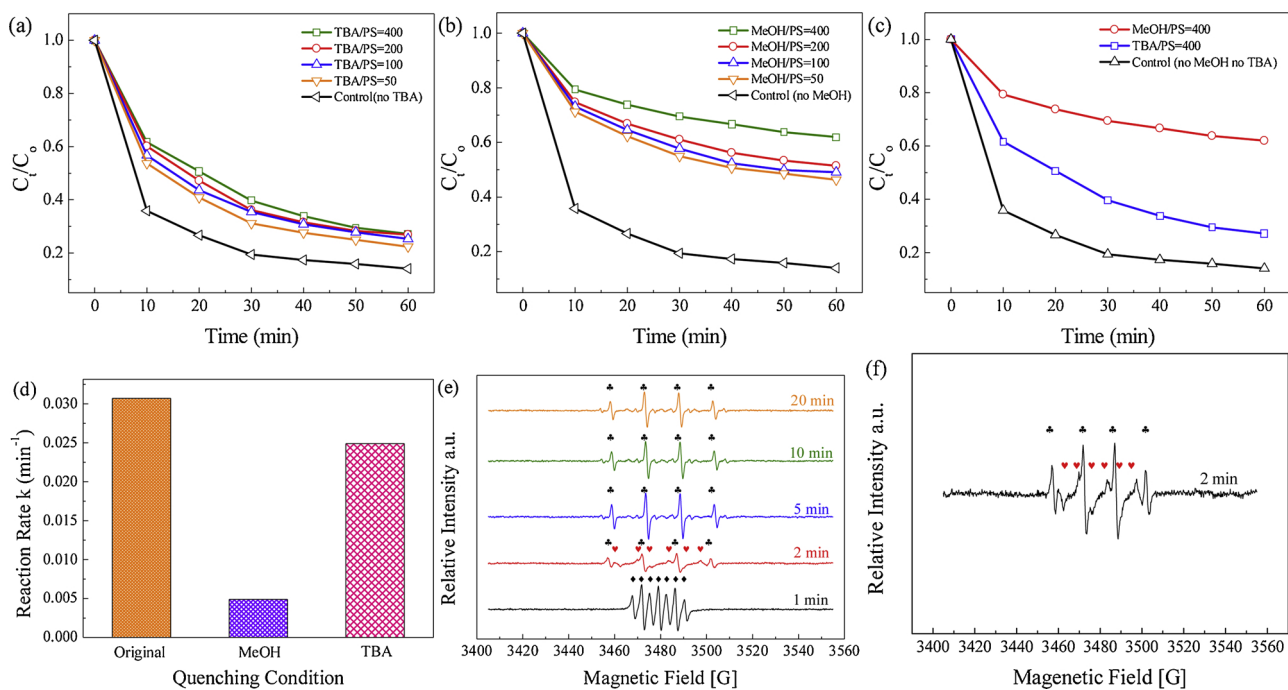


**Fig. 11.** Effects of (a) TBA and (b) MeOH on OFX degradation at different molar ratio with PMS, [OFX] = 300 mg/L, catalyst loading = 1 g/L, [PMS] = 3 g/L, MW = 400 W, [Temp] = 50 °C. (c) Effects of TBA and MeOH on OFX degradation at 400 M ratio with PMS. (d) Changes of reaction rate (k) of catalysts with and without quenching agents of MeOH and TBA at 400 M ratio with PMS. (e) EPR spectra in various conditions. Centerfield: 3480 G; sweep width: 200 G; microwave frequency: 9.77 GHz; modulation frequency: 1 GHz; and power: 20 mW. Reaction condition: DMPO = 100 mmol/L, ◆: DMPO-·OH, ♦: DMPO-SO<sub>4</sub><sup>·-</sup>.

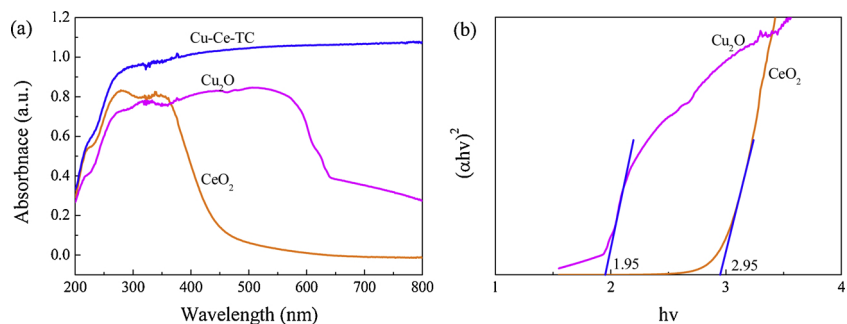


Fig. 12. UV-vis diffuse reflectance spectra (a); Plots of  $(\alpha h v)^2$  versus  $h v$  (b).

generated and took part in the reaction, while the dominant radical in the system is SO<sub>4</sub><sup>·-</sup>—rather than ·OH which is consistent with the previous reports.

In order to investigate the catalytic oxidation mechanism and further determine oxidative radicals have been involved in the reactions, EPR tests were carried out using Cu-Ce-TC as the catalyst and DMPO as the spin trapping agent. As shown in Fig. 11(e), at 1 min, characteristic signals with an intensity ratio of 1:2:1:2:1:2:1 were captured, which assigned to DMPO-·OH [65,66]. As shown in Fig. 11(f), characteristic signals of DMPO-·OH adducts (with hyperfine splitting constants of (aN = aH = 14.9 G) and DMPO-SO<sub>4</sub><sup>·-</sup>-adducts (with hyperfine splitting constants of (aN = 13.9 G, aH = 9.7 G, aH = 1.6 G and aH = 0.6 G) were observed at 2 min [64,65]. The signals of DMPO-·OH (1:2:2:1) and DMPO-SO<sub>4</sub><sup>·-</sup>-(1:1:1:1:1:1) revealed that both ·OH and SO<sub>4</sub><sup>·-</sup>-radicals were generated in the initial phase of the reaction [79]. And in the EPR spectra at 5 min, 10 min and 20 min, only signals of DMPO-·OH adducts were identified, due to sulfate radicals were more active than hydroxyl radicals in OFX degradation process. The intensity

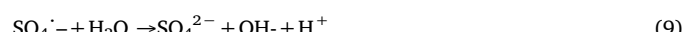
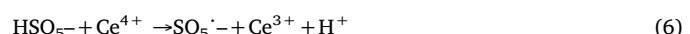
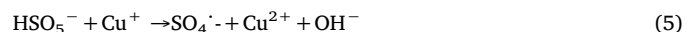
of DMPO-·OH decreased, which revealed the amount of ·OH was decreased in the process.

As reported in some studies, the p-n heterojunction that formed in different types of semiconductors can help electrons and holes separate more efficiently [67–70]. Copper oxide (Cu<sub>2</sub>O) has a narrow band gap and cerium dioxide (CeO<sub>2</sub>) has high carrier mobility and chemical and thermo stability due to oxygen vacancies and reversible Ce3p and Ce4p valence change [71,72]. The optical properties of as-prepared Cu-Ce-TC composites, pure Cu<sub>2</sub>O, CeO<sub>2</sub> and Cu-Ce-TC were analyzed by UV-vis diffuse reflectance spectra. As shown in Fig. 12(a), the absorption edge of Cu<sub>2</sub>O occurs at about 365 nm whereas absorption edge of the CeO<sub>2</sub> begins at about 550 nm, which correspond to band-gap energy of 1.95 and 2.95 eV, respectively in Fig. 12(b), which were similar to previous reports [71,73]. Remarkably, Cu-Ce-TC has a significant the absorbency compared with pure Cu<sub>2</sub>O and CeO<sub>2</sub>. Thus, Cu-Ce-TC composites exhibit better light capture capability and has a potential application in photocatalyst. Fig. 12(b) shows the linear transformation absorption curves for Cu<sub>2</sub>O and CeO<sub>2</sub>. The following formula is used to calculate the energy bandgap (Eg) [74]:

$$(\alpha h v)^2 = A(hv - Eg) \quad (4)$$

$\alpha$  and  $h v$  represent the absorbance and the energy of irradiation.

Based on the results, the mechanism of activation of PMS by Cu-Ce-TC for OFX degradation could be proposed as follows and shown in Fig. 13(a) and (b).



The effects of microwave activation include thermal and non-thermal effects [75]. Thermal effect is related to the heating of reaction environment [76]. In this study, the non-thermal effect of microwave activation may be remarkable. The OFX solution was degradation in PMS/Cu-Ce-TC/MW and PMS/Cu-Ce-TC/heat system. Temperature was controlled at 50 °C by microwave reactor and thermostat water bath, respectively. As shown in Fig. S3, 80.6% of OFX was degraded by the PMS/Cu-Ce-TC/MW process in 30 min, while only 48.2% of OFX was degraded by PMS/Cu-Ce-TC/heat in 30 min. The difference of degradation efficiency revealed that non-thermal effect of microwave activation exists in OFX degradation. Consistent with the previous reports, enhancement of electron transfer and increasing of reactants collision numbers are two potential mechanisms for the non-thermal effect of microwave activation [76]. Cu-Ce-TC could strongly absorb microwave and then generate numerous hotspots on the surface, which would speed up the movement of electrons. According to Eqs. (5) and (6), enhancement of electrons transfer would accelerate the generation of sulfate radicals. Moreover, the increased collision numbers between

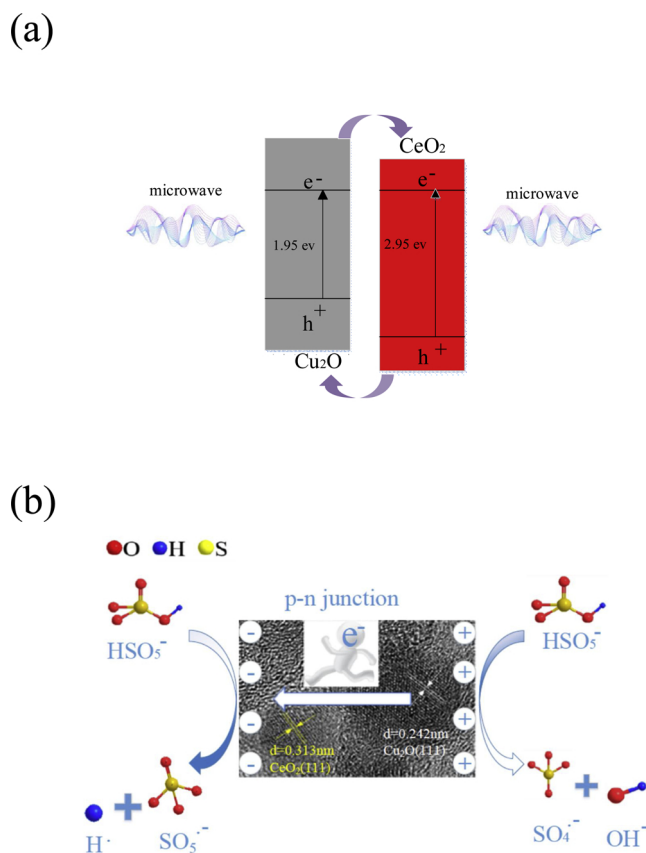


Fig. 13. The separation of photoexcited electrons and holes (a) and proposed mechanism of persulfate activation on Cu-Ce-TC (b).

OFX and  $\text{SO}_4^{2-}$  would be improved because microwave induced violent motion of reactants molecules.

#### 4. Conclusion

In summary, Cu-Ce-TC/MW/PMS system have great application potential in OFX wastewater treatment. This work not only provides a catalyst with high efficiency, stability and low price, but also gives an in-depth insight to the degradation intermediates/products and mechanism. A total of 11 intermediates/products of OFX were identified by GC-MS and HRMS. Five degradation pathways were proposed based on the results. This study demonstrated that  $\text{SO}_4^{2-}$  is the dominating active species in the system. The enhanced catalytic activities of Cu-Ce-TC might be attributed to the effective separation of electrons and holes with the help of p-n heterojunction. And microwave played an important role of electron transfer and increasing of reactants collision numbers in the persulfate activation process.

#### Acknowledgments

This work was funded by the Natural Science Foundation of Jiangsu Province (grant No. BK20160989), the Jiangsu Synergetic Innovation Center for Advanced Bio-Manufacture and the Natural Science Foundation of the Higher Education Institutions of Jiangsu Province, China (grant No. 16KJA610002).

#### Appendix A. Supplementary data

Supplementary material related to this article can be found, in the online version, at doi:<https://doi.org/10.1016/j.apcatb.2019.04.047>.

#### References

- [1] B.M. Padedda, et al., Consequences of eutrophication in the management of water resources in mediterranean reservoirs: a case study of lake cedrino (Sardinia, Italy), *Glob. Ecol. Conserv.* 12 (2017) 21–35.
- [2] W.G. Peng, Z. Xuan, S.G. Cai, Antibiotic wastewater treatment via advanced oxidation process, *Oxid. Commun.* 38 (2015) 1436–1442.
- [3] K.W. Goyne, et al., Sorption of the antibiotic ofloxacin to mesoporous and non-porous alumina and silica, *J. Colloid Interface Sci.* 283 (2005) 160–170.
- [4] C.C. Jara, et al., Electrochemical removal of antibiotics from wastewaters, *Appl. Catal. B: Environ.* 70 (1–4) (2007) 479–487.
- [5] R. Kaur, J.P. Kushwaha, N. Singh, Electro-oxidation of ofloxacin antibiotic by dimensionally stable Ti/RuO<sub>2</sub> anode: evaluation and mechanistic approach, *Chemosphere* 193 (2018) 685–694.
- [6] C. Rodrigues-Silva, et al., Occurrence and degradation of quinolones by advanced oxidation processes, *Quim. Nova* 37 (5) (2014) 868–885.
- [7] E. Hapeshi, et al., Drugs degrading photocatalytically: kinetics and mechanisms of ofloxacin and atenolol removal on titania suspensions, *Water Res.* 44 (6) (2010) 1737–1746.
- [8] M.S. Peres, M.G. Maniero, J.R. Guimaraes, Photocatalytic degradation of ofloxacin and evaluation of the residual antimicrobial activity, *Photochem. Photobiol. Sci.* 14 (3) (2015) 556–562.
- [9] A. Kaur, et al., Facile synthesis of CdS/TiO<sub>2</sub> nanocomposite and their catalytic activity for ofloxacin degradation under visible illumination, *J. Photochem. Photobiol. A* 360 (2018) 34–43.
- [10] A. Nikolaou, S. Meric, D. Fatta, Occurrence patterns of pharmaceuticals in water and wastewater environments, *Anal. Bioanal. Chem.* 387 (4) (2007) 1225–1234.
- [11] M.E. Grimmett, Removal of sulfamethazine by hypercrosslinked adsorbents in aquatic systems, *J. Environ. Qual.* 42 (1) (2013) 2–9.
- [12] C.Y. Zhou, et al., In situ grown AgI/Bi<sub>2</sub>O<sub>3</sub>/Cl<sub>2</sub> heterojunction photocatalysts for visible light degradation of sulfamethazine: efficiency, pathway, and mechanism, *ACS Sustain. Chem. Eng.* 6 (3) (2018) 4174–4184.
- [13] P. Avetta, et al., Activation of persulfate by irradiated magnetite: implications for the degradation of phenol under heterogeneous photo-Fenton-like conditions, *Environ. Sci. Technol.* 49 (2) (2015) 1043–1050.
- [14] X.Y. Chen, et al., Performance of nano-Co<sub>3</sub>O<sub>4</sub>/peroxymonosulfate system: kinetics and mechanism study using Acid Orange 7 as a model compound, *Appl. Catal. B: Environ.* 80 (1–2) (2008) 116–121.
- [15] E. Saputra, et al.,  $\alpha$ -MnO<sub>2</sub> activation of peroxymonosulfate for catalytic phenol degradation in aqueous solutions, *Catal. Commun.* 26 (2012) 144–148.
- [16] Y. Feng, et al., Efficient degradation of sulfamethazine with CuCo<sub>2</sub>O<sub>4</sub> spinel nanocatalysts for peroxymonosulfate activation, *Chem. Eng. J.* 280 (2015) 514–524.
- [17] Luís Gustavo Tdos Reis, et al., Separation of Malachite Green and Methyl Green cationic dyes from aqueous medium by adsorption on Amberlite XAD-2 and XAD-4 resins using sodium dodecylsulfate as carrier, *Chem. Eng. J.* 171 (2) (2011) 532–540.
- [18] R. Acosta, et al., Tetracycline adsorption onto activated carbons produced by KOH activation of tyre pyrolysis char, *Chemosphere* 149 (2016) 168–176.
- [19] O.S. Chan, et al., Preparation and characterisation of demineralised tyre derived activated carbon, *Carbon* 49 (14) (2011) 4674–4687.
- [20] T.A. Saleh, G.I. Danmaliki, Adsorptive desulfurization of dibenzothiophene from fuels by rubber tyres-derived carbons: kinetics and isotherms evaluation, *Process. Saf. Environ.* 102 (2016) 9–19.
- [21] O. Baytar, Investigation of high-activity activated carbon-supported Co-Cr-B Catalyst in the generation of hydrogen from hydrolysis of sodium borohydride, *Acta Chim. Slov.* 65 (2) (2018) 407–415.
- [22] E.G. Rodrigues, et al., Selective oxidation of glycerol catalyzed by Rh/activated carbon: importance of support surface chemistry, *Catal. Lett.* 141 (3) (2011) 420–431.
- [23] N. Katada, et al., Oxidation of sulfur dioxide to sulfuric acid over activated carbon catalyst produced from wood, *J. Jpn. Petrol. Inst.* 46 (6) (2003) 392–395.
- [24] R.B. Mathur, C. Lal, D.K. Sharma, Catalyst-free carbon nanotubes from coal-based material, *Energy Sources Part A* 29 (1) (2007) 21–27.
- [25] F. Mondragon, et al., The production of high surface carbons from coal using pre-swelling in solvents to disperse coking catalysts, *J. Mater. Sci.* 32 (6) (1997) 1455–1459.
- [26] H.J. Kim, et al., Enhanced activity and stability of TiO<sub>2</sub>-coated cobalt/carbon catalysts for electrochemical water oxidation, *ACS Catal.* 5 (6) (2015) 3463–3469.
- [27] S. Chornaja, et al., Pt supported TiO<sub>2</sub>-nanofibers and TiO<sub>2</sub>-nanopowder as catalysts for glycerol oxidation, *React. Kinet. Mech. Cat.* 119 (2) (2016) 569–584.
- [28] Q.L. Chen, et al., The promotion effect of Co doping on the K resistance of Mn/TiO<sub>2</sub> catalyst for NH<sub>3</sub>-SCR of NO, *J. Taiwan. Inst. Chem. E* 64 (2016) 116–123.
- [29] W. Pranee, et al., Dimethyl ether synthesis from methanol over diatomite catalyst modified using nitric acid treatment, *Energy Sources Part A* 38 (15) (2016) 2244–2249.
- [30] H. Liu, et al., Deactivation and regeneration of TS-1/diatomite catalyst for hydroxylation of phenol in fixed-bed reactor, *Chem. Eng. J.* 108 (3) (2005) 187–192.
- [31] E. Modiba, C. Enweremadu, H. Rutto, Production of biodiesel from waste vegetable oil using impregnated diatomite as heterogeneous catalyst, *Chin. J. Chem. Eng.* 23 (1) (2015) 281–289.
- [32] I. Michael-Kordatou, et al., On the capacity of ozonation to remove antimicrobial compounds, resistant bacteria and toxicity from urban wastewater effluents, *J. Hazard. Mater.* 323 (2017) 414–425.
- [33] M. Munoz, et al., Application of intensified Fenton oxidation to the treatment of sawmill wastewater, *Chemosphere* 109 (2014) 34–41.
- [34] A.C. Mecha, et al., Synergistic effect of UV-vis and solar photocatalytic ozonation on the degradation of phenol in municipal wastewater: a comparative study, *J. Catal.* 341 (2016) 116–125.
- [35] S. Miralles-Cuevas, et al., Removal of pharmaceuticals from MWTP effluent by nanofiltration and solar photo-Fenton using two different iron complexes at neutral pH, *Water Res.* 64 (2014) 23–31.
- [36] T. Paul, P.L. Miller, T.J. Strathmann, Visible-light-mediated TiO<sub>2</sub> photocatalysis of fluoroquinolone antibacterial agents, *Environ. Sci. Technol.* 41 (13) (2007) 4720–4727.
- [37] D.D. Qin, et al., Graphitic carbon nitride from burial to re-emergence on polyethylene terephthalate nanofibers as an easily recycled photocatalyst for degrading antibiotics under solar irradiation, *Accts Appl. Mater. Interface* 8 (39) (2016) 25962–25970.
- [38] Y.T. Lin, C.J. Liang, C.W. Yu, Trichloroethylene degradation by various forms of iron activated persulfate oxidation with or without the assistance of ascorbic acid, *Ind. Eng. Chem. Res.* 55 (8) (2016) 2302–2308.
- [39] R. Pulicharla, et al., Activation of persulfate by homogeneous and heterogeneous iron catalyst to degrade chlortetracycline in aqueous solution, *Chemosphere* 207 (2018) 543–551.
- [40] E. Neyens, J. Baeyens, A review of classic Fenton's peroxidation as an advanced oxidation technique, *J. Hazard. Mater.* 98 (1–3) (2003) 33–50.
- [41] X. Chen, et al., The role of miRNAs in drug resistance and prognosis of breast cancer formalin-fixed paraffin-embedded tissues, *Gene* 595 (2) (2016) 221–226.
- [42] G.P. Anipsitakis, D.D. Dionysiou, Degradation of organic contaminants in water with sulfate radicals generated by the conjunction of peroxymonosulfate with cobalt, *Environ. Sci. Technol.* 37 (20) (2003) 4790–4797.
- [43] C.Y. Sun, et al., Norcantharidin alone or in combination with crizotinib induces autophagic cell death in hepatocellular carcinoma by repressing c-Met-mTOR signaling, *Oncotarget* 8 (70) (2017) 114945–114955.
- [44] L. Tang, et al., Enhanced activation process of persulfate by mesoporous carbon for degradation of aqueous organic pollutants: electron transfer mechanism, *Appl. Catal. B: Environ.* 231 (2018) 1–10.
- [45] W.D. Oh, Z.L. Dong, T.T. Lim, Generation of sulfate radical through heterogeneous catalysis for organic contaminants removal: current development, challenges and prospects, *Appl. Catal. B: Environ.* 194 (2016) 169–201.
- [46] C.W. Luo, et al., Oxidation of the odorous compound 2,4,6-trichloroanisole by UV activated persulfate: kinetics, products, and pathways, *Water Res.* 96 (2016) 12–21.
- [47] Y.H. Guan, et al., Influence of pH on the formation of sulfate and hydroxyl radicals in the UV/peroxymonosulfate system, *Environ. Sci. Technol.* 45 (21) (2011) 9308–9314.
- [48] J.M. Monteagudo, et al., In situ chemical oxidation of carbamazepine solutions using persulfate simultaneously activated by heat energy, UV light, Fe<sup>2+</sup> ions, and H<sub>2</sub>O<sub>2</sub>, *Appl. Catal. B: Environ.* 176 (2015) 120–129.
- [49] Y.F. Ji, et al., Heat-activated persulfate oxidation of atrazine: implications for remediation of groundwater contaminated by herbicides, *Chem. Eng. J.* 263 (2015)

- 45–54.
- [50] C. Cai, et al., Ultrasound enhanced heterogeneous activation of peroxymonosulfate by a bimetallic Fe-Co/SBA-15 catalyst for the degradation of orange II in water, *J. Hazard. Mater.* 283 (2015) 70–79.
- [51] O.S. Furman, A.L. Teel, R.J. Watts, Mechanism of base activation of persulfate, *Environ. Sci. Technol.* 44 (16) (2010) 6423–6428.
- [52] M. Ahmad, A.L. Teel, R.J. Watts, Mechanism of persulfate activation by phenols, *Environ. Sci. Technol.* 47 (11) (2013) 5864–5871.
- [53] G.D. Fang, et al., Key role of persistent free radicals in hydrogen peroxide activation by biochar: implications to organic contaminant degradation, *Environ. Sci. Technol.* 48 (3) (2014) 1902–1910.
- [54] G.P. Anipsitakis, D.D. Dionysiou, Transition metal/UV-based advanced oxidation technologies for water decontamination, *Appl. Catal. B: Environ.* 54 (3) (2004) 155–163.
- [55] M.H. Nie, et al., Degradation of chloramphenicol by persulfate activated by  $\text{Fe}^{2+}$  and zerovalent iron, *Chem. Eng. J.* 279 (2015) 507–515.
- [56] Y.B. Kim, J.H. Ahn, Changes of absorption spectra, SUVA(254), and color in treating landfill leachate using microwave-assisted persulfate oxidation, *Korean J. Chem. Eng.* 34 (7) (2017) 1980–1984.
- [57] N.N. Patil, S.R. Shukla, Degradation of reactive yellow 145 dye by persulfate using microwave and conventional heating, *J. Water Process. Eng.* 7 (2015) 314–327.
- [58] S.Y. Yang, et al., A novel advanced oxidation process to degrade organic pollutants in wastewater: microwave-activated persulfate oxidation, *J. Environ. Sci.* 21 (9) (2009) 1175–1180.
- [59] G. Asgari, A. Seidmohammadi, A. Chavoshani, Pentachlorophenol removal from aqueous solutions by microwave/persulfate and microwave/ $\text{H}_2\text{O}_2$ : a comparative kinetic study, *J. Environ. Sci. Health* 12 (1) (2014) 94.
- [60] C.L. Jiang, et al., Sulfate radical-based oxidation of fluoroquinolone antibiotics: kinetics, mechanisms and effects of natural water matrices, *Water Res.* 106 (2016) 507–517.
- [61] Y.F. Ji, et al., Thermo activated persulfate oxidation of antibiotic sulfamethoxazole and structurally related compounds, *Water Res.* 87 (2015) 1–9.
- [62] H.B. Yu, et al., Preparation of  $\text{CeO}_2$ -quantum dots/ $\text{Cu}_2\text{O}$  nanocomposites with enhanced photocatalytic properties, *J. Nanosci. Nanotechno.* 18 (8) (2018) 5794–5798.
- [63] C. Rahil, et al., Assessment of reaction intermediates of gamma radiation-induced degradation of ofloxacin in aqueous solution, *Chemosphere* 208 (2018) 606–613.
- [64] L. Tang, et al., Enhanced activation process of persulfate by mesoporous carbon for degradation of aqueous organic pollutants: electron transfer mechanism, *Appl. Catal. B: Environ.* 231 (2018) 1–10.
- [65] Y. Wang, et al., 3D-hierarchically structured  $\text{MnO}_2$  for catalytic oxidation of phenol solutions by activation of peroxymonosulfate: structure dependence and mechanism, *Appl. Catal. B: Environ.* 164 (2015) 159–167.
- [66] G.M. Rosen, et al., Spin trapping of the primary radical involved in the activation of the carcinogen N-hydroxy-2-acetylaminofluorene by cumene hydroperoxide-hematin, *Mol. Pharmacol.* 17 (1980) 233–238.
- [67] H.B. Yu, et al., Photocatalytic degradation of malathion in aqueous solution using an Au-Pd-TiO<sub>2</sub> nanotube film, *J. Hazard. Mater.* 184 (1–3) (2010) 753–758.
- [68] J. Yang, et al., A top-down strategy towards monodisperse colloidal lead sulphide quantum dots, *Nat. Commun.* 4 (2013) 1695.
- [69] D.M. Zhang, et al., Essential roles of defects in pure graphene/ $\text{Cu}_2\text{O}$  photocatalyst, *Catal. Commun.* 76 (2016) 7–12.
- [70] D.F. Zhang, et al., Delicate control of crystallographic facet-oriented  $\text{Cu}_2\text{O}$  nanocrystals and the correlated adsorption ability, *J. Mater. Chem.* 19 (29) (2009) 5220–5225.
- [71] L. Xu, et al., Synergy effect over electrodeposited submicron  $\text{Cu}_2\text{O}$  films in photocatalytic degradation of methylene blue, *Appl. Surf. Sci.* 258 (2012) 4934–4938.
- [72] Z. Li, et al., Sustainable synthesis of  $\text{CeO}_2$ /CdS-diethylenetriamine composites for enhanced photocatalytic hydrogen evolution under visible light, *J. Alloys Compd.* 758 (2018) 162–170.
- [73] F. Jiang, et al., Enhancement of photocatalytic decomposition of perfluoroctanoic acid on  $\text{CeO}_2/\text{In}_2\text{O}_3$ , *RSC Adv.* 6 (2016) 72015–72021.
- [74] Z. Wang, et al., Plasmonic  $\text{Ag}_2\text{MoO}_4/\text{AgBr}/\text{Ag}$  composite excellent photo-catalytic performance and possible photocatalytic mechanism, *Appl. Surf. Sci.* 396 (2017) 791–798.
- [75] N. Remya, et al., Current status of microwave application in wastewater treatment—a review, *Chem. Eng. J.* 166 (2011) 797–813.
- [76] Y. Pang, H. Lei, Degradation of p-nitrophenol through microwave-assisted heterogeneous activation of peroxymonosulfate by manganese ferrite, *Chem. Eng. J.* 287 (2016) 585–592.
- [77] An. Taicheng, et al., Kinetics and mechanism of advanced oxidation processes (AOPs) in degradation of ciprofloxacin in water, *Appl. Catal. B: Environ.* 94 (2010) 3–4.
- [78] An. Taicheng, et al., Mechanistic considerations for the advanced oxidation treatment of fluoroquinolone pharmaceutical compounds using TiO<sub>2</sub> heterogeneous catalysis, *J. Phys. Chem. A* 114 (2010) 2569–2575.
- [79] Wanjun Wang, et al., Catalyst-free activation of persulfate by visible light for water disinfection: efficiency and mechanisms, *Water Res.* 157 (2019) 106–118.